Spin dynamics of two-coupled nanomagnets in spin-flop tunnel junctions

A. Konovalenko,[1] E. Lindgren,[1] S. S. Cherepov,[1] V. Korenivski,[1] and D. C. Worledge[2]
[1]*Nanostructure Physics, Royal Institute of Technology, 10691 Stockholm, Sweden*
[2]*IBM T. J. Watson Research Center, Yorktown Heights, New York 10598, USA*
(Received 23 July 2009; published 29 October 2009)

Collective spin dynamics of two dipole-coupled nanomagnets in spin-flop tunnel junctions are studied experimentally and theoretically. The measured GHz magnetization oscillations reveal several collective spin-precessional modes. Analytical macrospin and numerical micromagnetic models of the spin-flop dynamics are developed, which provide a detailed explanation of the observed frequency spectra in terms of optical, acoustical, and micromagnetic modes in the antiparallel, parallel, and scissor magnetization states of the junctions.

DOI: 10.1103/PhysRevB.80.144425 PACS number(s): 85.75.Bb, 75.47.−m, 76.50.+g, 85.70.Kh

I. INTRODUCTION

The magnetization dynamics of a single ferromagnetic nanoparticle induced by external fields are well understood. They are governed by the Landau-Lifshitz-Gilbert (LLG) equation, which describes a spin precession with the resonance frequency determined by the effective anisotropy field of the particle.[1,2] The spin dynamics of *two nanomagnets* coupled by exchange and/or dipolar forces is, however, practically unexplored. In this two-particle case one should expect collective precessional modes to replace the single particle resonances when the interparticle coupling strength is comparable to or exceeds the single particle magnetic anisotropy energy. Such collective spin-wave modes have been the topic of strong interest in continuous magnetic multilayers and spatially extended heterostructures.[3–5] Indirect evidence for collective modes driven by spin torque has recently been inferred from noise measurements on synthetic ferrimagnets based on two exchange-coupled macrospins in nanopillar spin-valves.[6] The fundamental interest in the dynamics of *spin-flop* nanostructures, synthetic antiferromagnets based on two dipole-coupled macrospins in nanopillar tunnel junctions (TJ), is further enhanced by the significant advantages the structure offers for solid-state memory applications.[7] However, while *dynamic* switching has started to be simulated,[8,9] experimental investigations to date[10–13] focused exclusively on the *quasistatic* properties of the spin-flop system.

In this paper, we report on real-time and spectroscopic measurements of the dynamic magnetoconductance of nanosized spin-flop tunnel junctions in response to GHz field excitations. We show that the two-coupled nanomagnets, when dynamically excited by an external magnetic field, resonate in a collective fashion with the two main eigenmodes corresponding to particular azimuthal and polar motion of the two macrospins. The presence of two precessional eigenmodes in the spin-flop system is supported by a theoretical analysis of the two-particle LLG dynamics in the macrospin approximation. We derive analytical expressions for the eigenfrequencies, which agree well with the experimentally measured ones in the low and high-field limits, where the two moments are nearly antiparallel or parallel. Additionally, we observe complex multimode oscillations in the noncollinear (scissor) state of the devices, which are well-explained by our micromagnetic analysis of nonuniform spin distributions in the structure in the intermediate-field range.

II. EXPERIMENTAL DETAILS

A. Samples

The data presented in this paper are for elliptical tunnel junctions with 350×420 nm to 400×490 nm lateral dimensions. The spin-flop bilayer, illustrated in Fig. 1(a), is composed of nominally 6 nm thick $Ni_{81}Fe_{19}$ free layers separated by a 1-nm-thick TaN spacer, for which there is no interlayer exchange coupling, $J=0$. The effective magnetic thickness of the free layers, taking into account magnetically 'dead layers' at the surfaces,[14] was approximately 5 nm. An AlO_x tunnel barrier separates the bottom free layer and the pinned reference layer, composed of an artificial antiferromagnet (AAF). The typical resistance of the junctions used in this work was ~1 kΩ and the tunneling magnetoresistance $\sim20\%$. More details on the sample fabrication and characterization can be found in Refs. 13 and 14.

B. Measurement setup

All measurements were performed at room temperature. The on-chip integrated 50 Ω write and read lines were contacted using surface probes with 0–40 GHz bandwidth. An external magnetic field applied along the easy axis, H_{ea}, was used to produce various static parallel (P), antiparallel (AP), and scissor configurations of the two macrospins, which generally form arbitrary angles with respect to the easy axis [θ_1 and θ_2 in Fig. 1(b)].

The schematic of the apparatus for high speed measurements is shown in Fig. 1(c). The on-chip integrated write and read lines were contacted using Cascade surface probes with dc–40 GHz bandwidth. 100-ps range field pulses and GHz range continuous wave signals were used to dynamically excite the junctions. The write lines were designed to have 50 Ω resistance. The bandwidth of the driving circuit was estimated to be substantially higher than 6 GHz—the highest frequency used in this work. A 5 GS/s arbitrary waveform generator, Tektronix® AWG7052, was used to produce write line pulse signals with rise time of ~80 ps. A 0.1–20 GHz signal source was used to generate continuous wave signals. For quasistatic readout the junctions were current biased with $50-100$ μA and the voltage across the junctions was measured using a digital multimeter, for various external static field configurations.

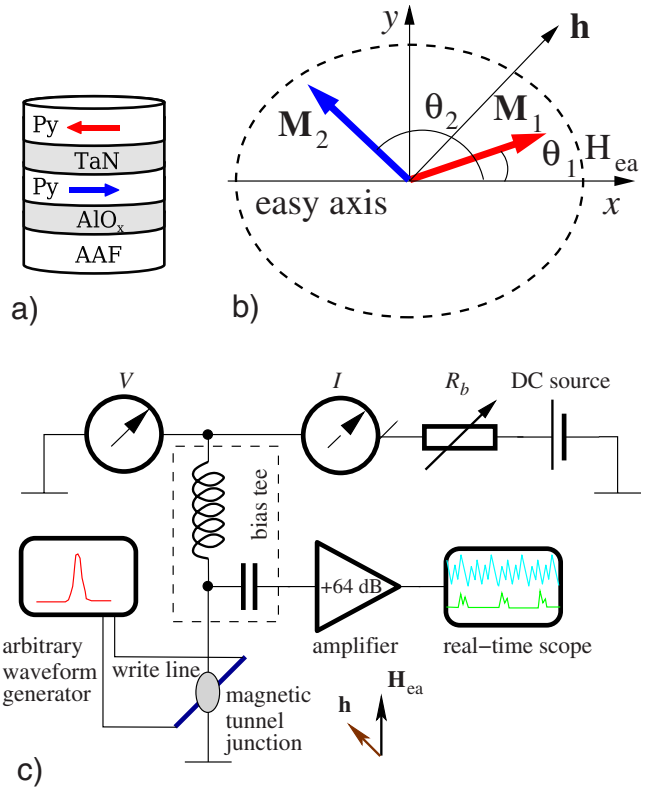

FIG. 1. (Color online) (a) Spin-flop tunnel junction: TJ magnetoresistance is due to rotations of bottom Py (blue arrow) relative to hard-pinned AAF; spin dynamics are due to coupled top and bottom Py particles (red and blue macrospins). (b) Illustration of a spin-flop bilayer with the two moments bent in-plane (optical mode) in response to ac field, h, applied at 45° to the easy axis. (c) Electrical circuit used for high speed measurements of the magnetization dynamics in spin-flop tunnel junctions: R_b is the bias resistance, V and I are the static voltage and current across the magnetic tunnel junction measured by digital multimeters. The ac voltage generated by the junction after excitation by the write line was amplified and recorded on a real-time oscilloscope.

For reading out the dynamic contribution to the junction voltage, a bias tee was used to separate the dc from the microwave signal, which was then amplified by +64 dB and recorded on a 40 GS/s Agilent® DSO80604B real-time oscilloscope with 6 GHz bandwidth. 5 ns long time traces were averaged 1024–4096 times to improve the signal to noise ratio. An electromagnet was used to produce various static parallel, antiparallel, and scissor configurations of the spin-flop bilayer. The external magnetic field H_{ea} was applied along the easy axis of the junctions. The pulse and continuous wave field excitation were applied through the write line, at 45° to the easy axis. The write line was not electrically connected to the junction.

C. Data processing for spectrograms

The ac voltage produced by the junction in response to field excitations (h) was recorded N times for a given magnetic field, H_{ea}, and subsequently averaged and current normalized to obtain the spectrograms of the ac voltage across

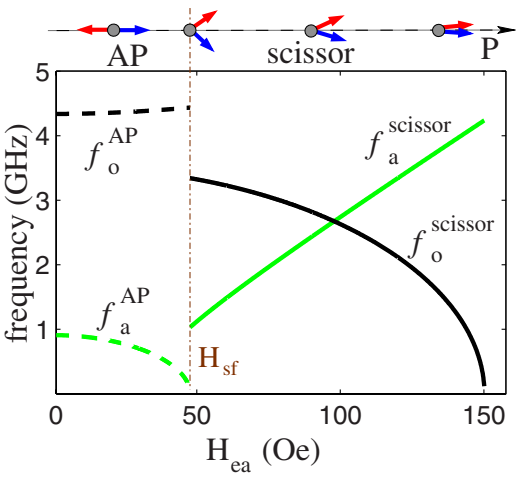

FIG. 2. (Color online) Theoretical spin-precessional modes of a spin-flop bilayer in the AP and scissor states versus the easy-axis field, predicted using a macrospin model: M_s=840 emu/cc, H_i =10 Oe, magnetic layer thickness 5 nm, lateral size 400 ×490 nm^2.

the junctions, $\langle V(t,H_{ea})\rangle$, such as shown in Fig. 3(b) below. For improving the resolution of the spectral peaks, a Hann window (Ref. 15, p. 553) was applied to each $\langle V(t,H_{ea})\rangle$ data set prior to the computation of the power spectral density (PSD), $PSD_{H_{ea}}(f)$. The PSD was computed (Ref. 15, p. 498) using the standard fast Fourier transform (FFT) $F(f,\langle V(t,H_{ea})\rangle)$

$$PSD_{H_{ea}}(f) = 2|F(f,\langle V(t,H_{ea})\rangle)|^2. \quad (1)$$

The full $PSD(f,H_{ea})$ spectral map, such as shown in Fig. 3(c) below, was obtained by stepping the field along the easy axis and repeating the above Hann-filtering and FFT procedure. The color scale corresponds to the resulting PSD amplitude.

In order to directly compare the experimental and theoretical spectra, the same procedure and code were used to compute the spectrograms from the micromagnetic simulations, such as shown in Fig. 5(c) below. The simulation results were converted into average magnetization angles for the two nanomagnets as functions of time, $\theta_{1,2}(t,H)$, for a given external magnetic field H. The PSD spectrograms of the resistance were then obtained from the simulated spin distributions using the angular dependence of the magnetoresistance, $R(\theta_1)\sim(1+P^2\cos\theta_1)^{-1}$,[16] and the FFT procedure detailed above. Here, θ_1 is the angle between the magnetization of the bottom free layer and the pinned reference layer, across the tunnel barrier, and P is the spin polarization. This results in the maximum magnetoresistive response to a small angle perturbation for $\theta_1\approx 100°$, i. e. in the scissor state. Spin oscillations in the AP state, at $H_{ea}<H_{sf}$, even though pronounced in amplitude, yield significantly weaker magnetoresistive signals.

III. MACROSPIN THEORY

The quasistatic magnetic phase diagram of a spin-flop junction is well-established.[7,17,18] Thus, for the external field

ramped up along the easy axis of the junction, a discontinuous spin-flop transition occurs at $H_{ea}=H_{sf}$ from the AP to the scissor magnetic state of the junction, as schematically shown in the top of Fig. 2. As the magnetic field is increased further, the magnetic moments gradually saturate toward the P state, resembling the action of scissors. Spin *dynamics* in spin-flop bilayers, on the other hand, remain unexplored. In this paper, we establish the necessary conceptual basis by first analyzing the spin dynamics for this system of two-coupled ferromagnetic particles in the macrospin approximation.

The total energy of the system, E, can be written as a sum of the energy terms describing the interactions in the system, such as the Zeeman energy, dipole-dipole interaction, demagnetizing terms, intrinsic anisotropy, and exchange coupling[17]

$$\begin{aligned} E(\theta_1,\theta_2)/VM_s = &- H_x(\cos\,\theta_1+\cos\,\theta_2) - H_y(\sin\,\theta_1+\sin\,\theta_2) \\ &+ (N_xM_s - j)\cos\,\theta_1\,\cos\,\theta_2 + (N_yM_s \\ &- j)\sin\,\theta_1\,\sin\,\theta_2 + \frac{1}{2}[(N_y-N_x)M_s + H_i] \\ &\times(\sin^2\,\theta_1+\sin^2\,\theta_2), \end{aligned} \tag{2}$$

where magnetic particle volume $V=\frac{1}{4}\pi abt$, demagnetization constants $N_{x,y}=4\pi n_{x,y}\frac{t}{b}$, $j=\frac{J}{tM_s}$, and $\theta_{1,2}$ are the angles of the two moments with respect to the easy-axis direction shown in Fig. 1(b), t is the thickness, a and b are the length and width of the ellipse along x and y, respectively, M_s is the saturation magnetization, J is the interlayer exchange coupling constant, and $H_{x,y}$ are the applied field components along x and y axes. The interlayer exchange coupling is negligible for the samples used in this work ($J=0$ for TaN spacers). Equation (2) is written for the case when both layers have the same thickness, i. e. there is no *thickness imbalance*. The x axis is the easy axis and the y axis is the in-plane axis normal to the easy axis. The expressions for demagnetizing factors $n_{x,y}$ are given in Ref. 17 and have relatively weak dependence on the ellipse aspect ratio a/b. Our typical samples have $a/b=1.2$, corresponding to $n_x\approx 0.62$ and $n_y \approx 0.82$. An assumption in Eq. (2) is that the dipole field outside one layer, acting on the other layer, is equal to the demagnetization field inside the first layer. This is justified in the case when the spacer between the two layers is thin. The expression for energy (2) can be used to obtain the spin-flop critical field, at which the system loses stability and spin-flops into the scissor state from the AP states $E(0,\pi)$ or $E(\pi,0)$. Similarly, the saturation field H_{xsat} can be derived from Eq. (2) for the easy-axis P state, $E(0,0)$, and the saturation field H_{ysat} can be derived from Eq. (2) for the hard-axis P state, $E(\pi/2,\pi/2)$. The final expressions for the main critical fields, H_{sf} and $H_{xsat,ysat}$ are[17]

$$H_{sf} = \sqrt{H_i\left(8\pi M_s n_y\frac{t}{b} - \frac{2J}{M_s t} + H_i\right)}, \tag{3}$$

$$H_{xsat} = 8\pi M_s n_x\frac{t}{b} - \frac{2J}{M_s t} - H_i, \tag{4}$$

$$H_{ysat} = 8\pi M_s n_y\frac{t}{b} - \frac{2J}{M_s t} + H_i. \tag{5}$$

We extend this quasistatic macrospin theory to model the dynamics of spin-flop tunnel junctions using two-coupled Landau-Lifshitz-Gilbert equations

$$\frac{d\mathbf{M}_{1,2}}{dt} = -|\gamma|\mathbf{M}_{1,2}\times\mathbf{H}^{\text{eff}}_{1,2} + \alpha\mathbf{M}_{1,2}\times\frac{d\mathbf{M}_{1,2}}{dt}, \tag{6}$$

where α is the damping parameter, and $\mathbf{H}^{\text{eff}}_{1,2}$ is the total effective field acting on each of the two ferromagnets, which can be computed from the total energy (2) of the system, $\mathbf{H}^{\text{eff}}_{1,2}=-\partial E(\theta_1,\theta_2)/\partial\mathbf{M}_{1,2}$.

The analytical expressions for the collective spin-precessional eigenmodes were derived by assuming small angle deviations from equilibrium and small damping, and solving Eq. (6) for its eigenfrequencies. These eigenfrequencies differ significantly in the AP and scissor states of the system:

$$\begin{aligned} &\text{I)}\quad 0\le H_{ea}<H_{SF},\ \text{(AP state)} \\ &\begin{cases} f_a^{AP}\approx\gamma\sqrt{H_{ea}^2-\sqrt{C_1H_{ea}^2+C_2}+C_3}, \\ f_o^{AP}\approx\gamma\sqrt{H_{ea}^2+\sqrt{C_1H_{ea}^2+C_2}+C_3}, \end{cases} \\ &\text{where} \\ &C_1 = 4(2\pi M_s+H_i)(2\pi M_s+H_i+N_yM_s-2j), \\ &C_2 = M_s^2(4\pi N_yM_s+N_yH_i-4\pi j)^2, \\ &C_3 = H_i^2+H_i[(N_y+4\pi)M_s-2j]+4\pi M_s(N_yM_s-j). \\ &\text{II)}\quad H_{SF}<H_{ea}<H_{xsat},\ \text{(scissor state)} \\ &\begin{cases} f_a^{\text{scissor}}\approx\gamma\sqrt{(4\pi M_s-2j)\left[\frac{H_{ysat}}{H_{xsat}^2}H_{ea}^2-H_i\right]}, \\ f_o^{\text{scissor}}\approx\gamma\sqrt{4\pi M_s\left[H_{xsat}-\frac{H_{ea}^2}{H_{xsat}}\right]}. \end{cases} \end{aligned} \tag{7}$$

Here γ=27.8 GHz/T, H_{ea} is the external field along easy axis, $H_{\{x,y\}sat}$ are the saturation fields defined by Eqs. (4) and (5), and constants $N_{x,y}$ and j are defined after Eq. (2). The four eigenfrequencies given by Eq. (7) are shown in Fig. 2 as a function of the easy-axis field.

For the special case of H_{ea}=0, [Eq. (7), case I] reduces to the following simple formulas for the acoustical and optical modes in the AP state:

$$f_a^{AP}(H_{ea}=0) \approx \gamma\sqrt{(4\pi M_s + H_i - 2j)H_i},$$

$$f_o^{AP}(H_{ea}=0) \approx \gamma\sqrt{(4\pi M_s + H_i)H_{ysat}}. \quad (8)$$

Substituting Eq. (5) into Eq. (8) with j=0 and assuming $H_i \ll 4\pi M_s$ leads to the following experimentally verifiable dependence of the optical eigenmode frequency $f_o^{AP}(b, H_{ea}=0)$ on the width of the junction, b

$$f_o^{AP} \approx 4\pi\gamma M_s \sqrt{2n_y \frac{t}{b}} \sim b^{-1/2}. \quad (9)$$

The acoustical f_a^{AP} mode consists of azimuthal bodily rotation (restoring force is intrinsic anisotropy, H_i) with polar bending, and the optical f_o^{AP} mode consists of azimuthal bending (restoring force is dipole and demag fields represented by the saturation field along the hard axis, H_{ysat}) with polar bodily rotation. Note that in both cases the restoring force for the polar motion is the large $4\pi M_s$ demagnetization field, which forces the precession trajectories to be largely in-plane.

In the scissor state, above the spin-flop point [case II in Eq. (7)], the acoustical mode consists of both azimuthal and polar bodily rotation; the two moments maintain a fixed angle between them as they precess. The optical mode consists of both azimuthal and polar bending. The two eigenmodes in the scissor state have a distinctly different dependence on increasing field: the frequency of the optical mode decreases since the applied field helps to saturate the moments thereby reducing the restoring force of the dipole and demag fields represented by the saturation field along the easy axis, H_{xsat}, while that of the acoustical mode increases (just like that for a single layer) as the applied field H_{ea} binds the moments more strongly to the easy axis. Our macrospin analysis shows that the two eigenmodes cross in the scissor state prior to saturation, as shown in Fig. 2.

We have also directly numerically integrated Eq. (6). After performing a spectral analysis of the solutions obtained from Eq. (6), we identified peaks in the spectra as corresponding to resonant eigenmodes at acoustical (f_a) and optical (f_o) frequencies. These numerically obtained modes are in excellent agreement with the analytical expressions for $f_{o,a}(H_{ea})$ derived below. The power spectral density of $\theta_{1,2}(t)$ and $M_{1,2}^{x,y}(t)$ are essentially the same in the two cases.

IV. EXPERIMENTAL RESULTS AND DISCUSSION

The spin-flop point, H_{sf}, separates two regions in field, AP and scissor, where a spin-flop bilayer is expected to show distinctly different behavior. To determine the H_{sf} point experimentally we initialize a junction into the AP state and measure its resistance, while gradually increasing the field along the easy axis. The two moments remain antiparallel until $H_{ea}=H_{sf}$, where they discontinuously jump into the scissor state, as shown in Fig. 3(a). The resistance is nearly constant for fields $H_{ea}<H_{sf}$. At H_{sf}=46 Oe, the resistance changes abruptly by a significant fraction of the magnetoresistance, which reflects the large deviation of the scissored bottom layer (interfacing the tunnel barrier) from the easy axis. The subsequent increase in the field toward the saturation field, H_{xsat}, gradually aligns the two layers (via several small discrete steps, to be discussed in detail later) such that the tunnel junction resistance approaches the original state.

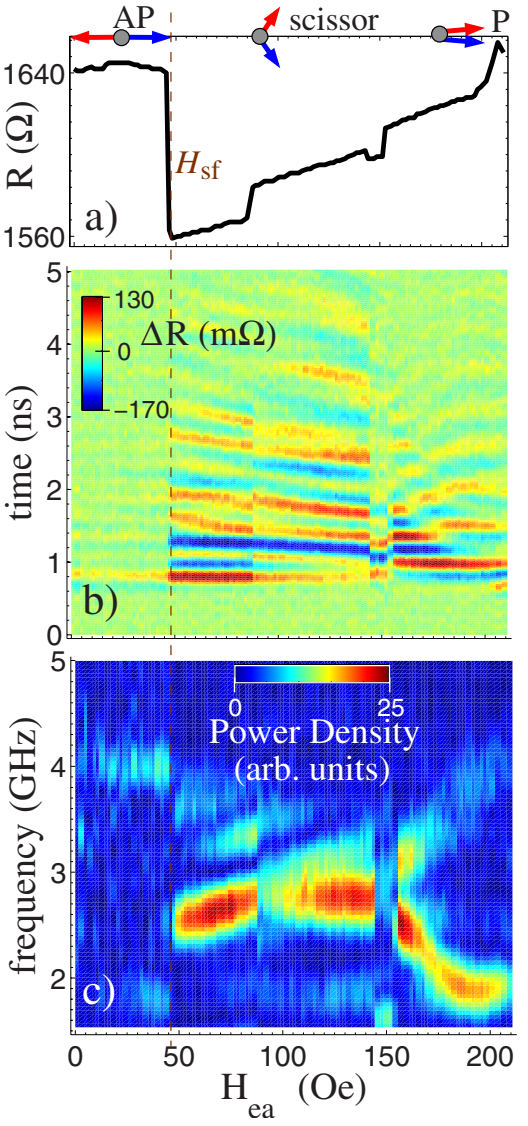

FIG. 3. (Color online) Static resistance (a), dynamic magnetoresistance (b) and its frequency spectrum (c), for a 400×490 nm^2 junction as a function of the easy-axis field.

We magnetically excite the free layers by applying 80 ps rise/fall time, 200 ps wide in-plane field pulses of h =10–30 Oe in amplitude. The color scale in Fig. 3(b) shows a typical real-time trace of the oscillations in resistance following such a field pulse, measured for a range of static H_{ea} from 0 to 220 Oe. Weakly detected oscillations in the AP

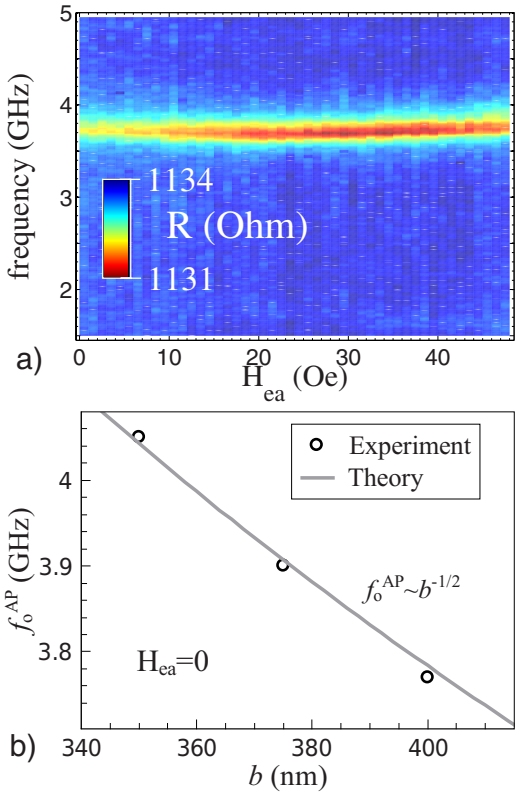

FIG. 4. (Color online) (a) $R(f,H_{ea})$ spectral map measured as a response to 10 Oe ac excitation, for a 400×490 nm^2 junction, in the AP state. The junction used in this measurement has the same nominal size and a slightly thinner tunnel barrier compared to the junction used in Fig. 2. (b) Optical eigenfrequency $f_o^{AP}(H_{ea}=0)$ as a function of the junction width b for a fixed aspect ratio of 1.2 (each data point is the average of f_o^{AP} for two junctions of the same size). Solid line in (b) is the macrospin theory fit using the nominal $M_s=840$ emu/cc, $H_i=10$ Oe, $b=400$ nm, aspect ratio=1.2, and $t_{fit}=3.8$ nm.

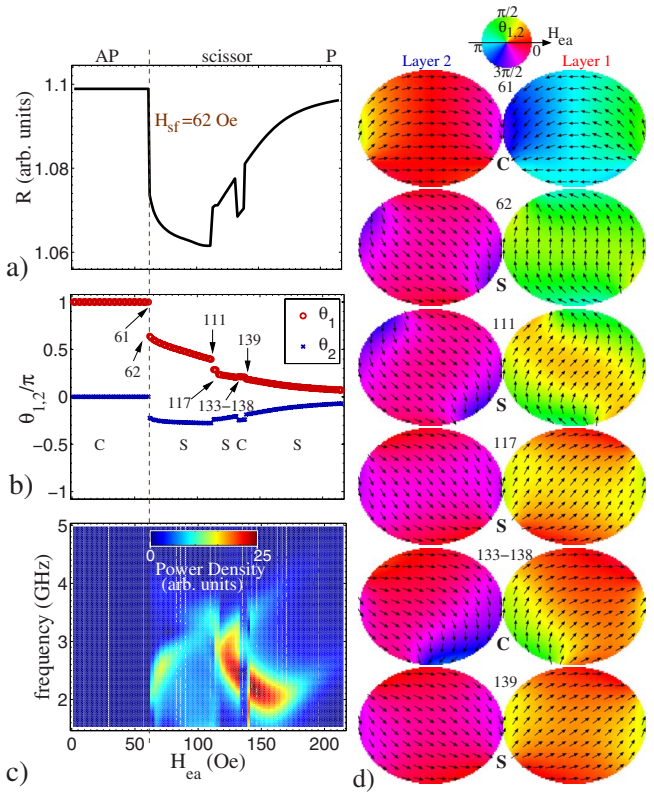

FIG. 5. (Color online) Micromagnetic simulation of the spin-flop dynamics for a 400×490 nm^2 junction: (a) resistance versus H_{ea}; (b) average angles of the two magnetic particles versus H_{ea}; (c) frequency spectrum of the junction resistance in response to a 200 ps 20 Oe pulse; (d) nonuniform spin distributions within the top (layer 1) and bottom (layer 2) ferromagnetic layers at H_{ea} values corresponding to micromagnetic transition between the *C*- and *S*-shaped spin distributions in the structure.

state are followed by a distinct transition to strong magnetoresistive oscillations in the scissor state,[16] with several abrupt bands versus H_{ea}, which correlate precisely with the steplike transitions in the static resistance shown in (a). The frequency spectrum in Fig. 3(c) shows, in the AP state, a weakly visible optical mode at approximately 4 GHz, and a trace of the acoustical mode between 1.5 and 2 GHz at $H_{ea}\approx H_{sf}$. At $H_{ea}>H_{sf}$, there is an abrupt transition to several pronounced multimodes and bands. The spectrum then transforms into what appears to be the optical-acoustical crossover at ~150 Oe, with the two modes diverging in frequency, in good agreement with the predicted behavior shown in Fig. 2.

In order to increase the experimental resolution in detecting the magnetoresistive oscillations in the AP state, a spectroscopic measurement technique was used, in which the junctions were excited using a small-signal ac hard-axis field and the resistance was monitored quasistatically. As the ac frequency is swept from sub-GHz to 5 GHz, resonant spin excitations are expected at the eigenfrequencies of the spin-flop bilayer, accompanied by large (resonant) spin deviations from the easy axis and therefore peaks in $R(f)$. This is indeed observed, as shown in Fig. 4(a).

It is important to note that the spin excitations in this case are *forced* by the ac field, in contrast to the *free* spin oscillations following short pulses used in the real-time measurements of Fig. 3. Therefore, the optical (bending) mode at ~4 GHz, where the two macrospins naturally follow the driving ac field, is expected to dominate. Only traces of the acoustical mode are seen at ~1 GHz near H_{sf} (not visible), which is to be expected since the driving ac field disfavors the fixed-angle in-plane rotation involved. The dependence of the optical mode frequency measured at zero field on the junction width b is shown in Fig. 4(b) and agrees well with a fit to Eq. (9) where we varied one parameter, the thickness. The fit value $t_{fit}=3.8$ nm suggests a smaller than expected moment, consistent with a dead layer and also curling of the magnetization along the edges, as seen in micromagnetic simulations [see the top panel of Fig. 5(d)]. Thus, the spin-flop dynamics in the AP state is single-domain-like, with a reduced effective moment, owing to the relatively strong dipole coupling stabilizing the uniform spin distribution even for junction sizes exceeding the macrospin limit.

V. MICROMAGNETIC MODEL RESULTS

Figure 5 provides a detailed micromagnetic interpretation of the observed spin dynamics for the entire field range.[19]

The AP state at low H_{ea} [(d) top, H_{ea}=61 Oe] shows only small spin perturbations and therefore the spectrum is macrospinlike.

The spin-flop transition at 62 Oe produces a highly asymmetric scissor state of the bilayer, as can be clearly seen in (d) and by comparing the average θ_1 and θ_2 in (b). Summing over the *C*-shaped spin distributions shown in the top panel of (d) indicates that layer 2 has a slightly larger effective moment in the AP state and therefore the spin-flop transition results in layer 2 aligned with the field, analogous to a direct write in the single-domain model.[17] Layer 1, aligned quite asymmetrically with respect to the easy axis, is gradually rotated toward the easy axis as the field increases to approximately 110 Oe. The spins in the center of layer 1 can rotate more easily than the spins at the edges, because of the large demag fields at the edges, which results in a distinct *S*-shaped spin profile at 111 Oe. At 117 Oe the edges of the layers switch, resulting in discontinuous changes in θ_1 and θ_2 and a micromagnetically different *S*-shaped profile. Then, at 133–138 Oe, the bottom edge of layer 2 switches, putting the layers into a predominantly *C*-shaped spin state. Eventually, at fields >139 Oe, the layers form almost saturated *S*-shaped spin distributions. The two layers follow these *C*-*S*-*C*-*S* transitions synchronously due to the strong dipole coupling between the layers. The micromagnetic changes in the spin distribution of layer 2 are weaker, however, since it is already aligned roughly with the easy axis field above the spin-flop point. The abrupt micromagnetic transitions at 112, 117, 133, and 139 Oe lead to sharp changes in the average angles (b) and new bands in the frequency spectrum shown in (c). The scissor state is asymmetric and highly nonuniform in this field range of 62–138 Oe, which results in the spectrum being quite different from the macrospin prediction. The micromagnetic transition at 139 Oe brings the bilayer into a rather symmetric, quasiuniform state (b), (d). In this high-field scissor state the spectrum resembles the expected macrospin optical-acoustical cross, Fig. 2. This micromagnetic interpretation is in excellent agreement with the experimental data of Fig. 3(c).

VI. CONCLUSIONS

Collective optical and acoustical spin-precessional modes are observed in spin-flop tunnel junctions in the 1–5 GHz range. The field dependence of the spin oscillation frequencies in the AP state and the high-field scissor state are in good agreement with the macrospin model. Micromagnetic simulation shows that the observed complex, multimode spectra in the intermediate-field scissor state are well-explained by hopping between several near-degenerate *C* and *S* nonuniform spin states.

ACKNOWLEDGMENTS

We thank the IBM MRAM team for sample fabrication. This work was supported by the Swedish funding agency SSF, K. A. Wallenberg and G. Gustafsson foundations, and the IBM Faculty Grant 2007–2008.

[1] R. H. Koch, J. G. Deak, D. W. Abraham, P. L. Trouilloud, R. A. Altman, Y. Lu, W. J. Gallagher, R. E. Scheuerlein, K. P. Roche, and S. S. P. Parkin, Phys. Rev. Lett. **81**, 4512 (1998); R. H. Koch, G. Grinstein, G. A. Keefe, Y. Lu, P. L. Trouilloud, W. J. Gallagher, and S. S. P. Parkin, *ibid.* **84**, 5419 (2000).

[2] J. C. Siegmann, *Magnetism: From Fundamentals to Nanoscale Dynamics*, Springer Series in Solid-State Sciences Vol. 152, edited by J. Stöhr and H. C. Siegmann (Springer, New York, 2006), XVIII, 820, p. 325, ISBN: 978-3-540-30282-7.

[3] M. Belmeguenai, T. Martin, G. Woltersdorf, M. Maier, and G. Bayreuther, Phys. Rev. B **76**, 104414 (2007).

[4] N. I. Polushkin, S. A. Michalski, L. Yue, and R. D. Kirby, Phys. Rev. Lett. **97**, 256401 (2006); N. I. Polushkin, Phys. Rev. B **77**, 180401(R) (2008).

[5] M. Buchmeier, H. Dassow, D. E. Burgler, and C. M. Schneider, Phys. Rev. B **75**, 184436 (2007).

[6] N. Smith, S. Maat, M. J. Carey, and J. R. Childress, Phys. Rev. Lett. **101**, 247205 (2008).

[7] B. N. Engel *et al.*, IEEE Trans. Magn. **41**, 132 (2005).

[8] D. Cimpoesu *et al.*, J. Appl. Phys. **102**, 013915 (2007).

[9] S. Wang *et al.*, IEEE Trans. Magn. **43**, 2337 (2007).

[10] T. Yamamoto *et al.*, J. Appl. Phys. **97**, 10P503 (2005).

[11] Y. Fukumoto *et al.*, J. Appl. Phys. **103**, 013902 (2008).

[12] V. Korenivski *et al.*, Appl. Phys. Lett. **86**, 252506 (2005).

[13] D. C. Worledge *et al.*, J. Appl. Phys. **100**, 074506 (2006).

[14] D. W. Abraham *et al.*, IBM J. Res. Dev. **50**, 55 (2006).

[15] W. H. Press, S. A. Teukolsky, W. T. Vetterling, and B. P. Flannery, *Numerical Recipes in C: The Art of Scientific Computing*, 2nd ed. (Cambridge University Press, Cambridge, England, 1992).

[16] J. C. Slonczewski, Phys. Rev. B **39**, 6995 (1989).

[17] D. C. Worledge, Appl. Phys. Lett. **84**, 2847 (2004); **84**, 4559 (2004); IBM J. Res. Dev. **50**, 69 (2006).

[18] H. Fujiwara *et al.*, J. Appl. Phys. **97**, 10P507 (2005).

[19] Results obtained using OOMMF: M. J. Donahue and D. G. Porter, OOMMF user's guide, NIST-MD, http://math.nist.gov/oommf